Awan, Hafiz Asad Ali; Hinkkanen, Marko; Bojoi, Radu; Pellegrino, Gianmario

Stator-flux-oriented control of synchronous motors

Published in:
Proceedings of the 10th IEEE Energy Conversion Congress and Exposition, ECCE 2018

DOI:
10.1109/ECCE.2018.8557667

Published: 23/09/2018

Document Version
Peer-reviewed accepted author manuscript, also known as Final accepted manuscript or Post-print

Please cite the original version:
Awan, H. A. A., Hinkkanen, M., Bojoi, R., & Pellegrino, G. (2018). Stator-flux-oriented control of synchronous motors: Design and implementation. In *Proceedings of the 10th IEEE Energy Conversion Congress and Exposition, ECCE 2018* (pp. 6571-6577). (IEEE Energy Conversion Congress and Exposition). IEEE. https://doi.org/10.1109/ECCE.2018.8557667

Stator-Flux-Oriented Control of Synchronous Motors: Design and Implementation

Hafiz Asad Ali Awan*, Marko Hinkkanen*, Radu Bojoi†, and Gianmario Pellegrino†
*Aalto University, Espoo, Finland
†Politecnico di Torino, Turin, Italy

***Abstract*—This paper deals with a stator-flux-oriented control method for permanent-magnet (PM) synchronous motors and synchronous reluctance motors (SyRMs). The stator-flux magnitude and the torque-producing current component are the controlled variables. This choice simplifies the references calculation (as compared to the current control in rotor coordinates), but the dynamics seen by the inner control loops become nonlinear and coupled, potentially compromising the control performance. We propose an exact input-output feedback linearization structure and a systematic design procedure for the stator-flux-oriented control method. Simulation and experimental results are presented to verify the dynamic performance of the designed controller using a 6.7-kW SyRM drive.**

***Index Terms*—Input-output feedback linearization, nonlinear control, stator-flux-oriented control, permanent-magnet synchronous motor, synchronous reluctance motor.**

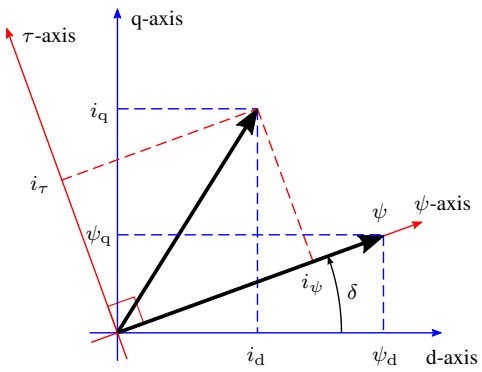

Fig. 1. Rotor coordinates (dq) and stator-flux coordinates ($\psi\tau$). Flux and current components are depicted in both coordinates.

I. Introduction

Synchronous reluctance motors (SyRMs) with or without permanent magnets (PMs) provide high torque density, good flux-weakening capability, and wide constant power region. Under optimal control, these motors operate along the maximum-torque-per-ampere (MTPA) locus, in the field-weakening region, or at the maximum torque-per-volt (MTPV) limit, depending on the operating speed and the torque reference.

Many control schemes are based on controlling the current vector in rotor coordinates [1]–[3]. If the magnetic saturation and the speed changes are omitted, the dynamics seen by the current controller are linear and the closed-loop system can be made comparatively robust [3]. The optimal current references can be fetched from pre-computed look-up tables [2], [4]. In addition to one-dimensional MTPA and MTPV tables, at least one two-dimensional look-up table is typically needed.

In stator-flux-oriented control [5] and in its variant called direct-flux vector control (DFVC) [6], [7], the stator-flux magnitude and the torque-producing current component are selected as the controlled variables. This choice simplifies the reference calculation, since only the MTPA and MTPV features have to be implemented, while no two-dimensional look-up tables are needed. Typically, two separately tuned proportional-integral (PI) controllers are used for controlling the stator-flux magnitude and the torque-producing current component [6]–[8]. Instead of controlling the torque-producing current component, it is also possible to control the electromagnetic torque directly [9].

A drawback of these stator-flux-oriented schemes is that the torque-producing current control loop becomes nonlinear (even in the case of linear magnetics), which complicates the tuning procedure. The control perfomance for constant gains depends on the operating point due to the nonlinear dynamics. To avoid an oscillatory response, the control design can be performed for the worst case in a suboptimal manner [6].

In this paper, we develop a modified stator-flux-oriented control method, using the methods in [5]–[7] as a starting point. After presenting the motor model in rotor and stator-flux coordinates in Section II, the control structure and the main contributions are presented in Section III:

1) An exact input-output feedback linearization controller structure is derived, yielding a completely decoupled system;
2) A state-feedback controller with integral action and reference feedforward is designed;
3) Design guidelines and tuning principles are presented;
4) The anti-windup mechanism is developed, taking into account the nonlinear structure of the controller.

We will also show that the flux observer is not necessary, even thought it can be useful in practice. To verify the dynamic performance of the designed controller, simulations and experiments are performed for a 6.7-kW SyRM drive and the results are presented in Section IV.

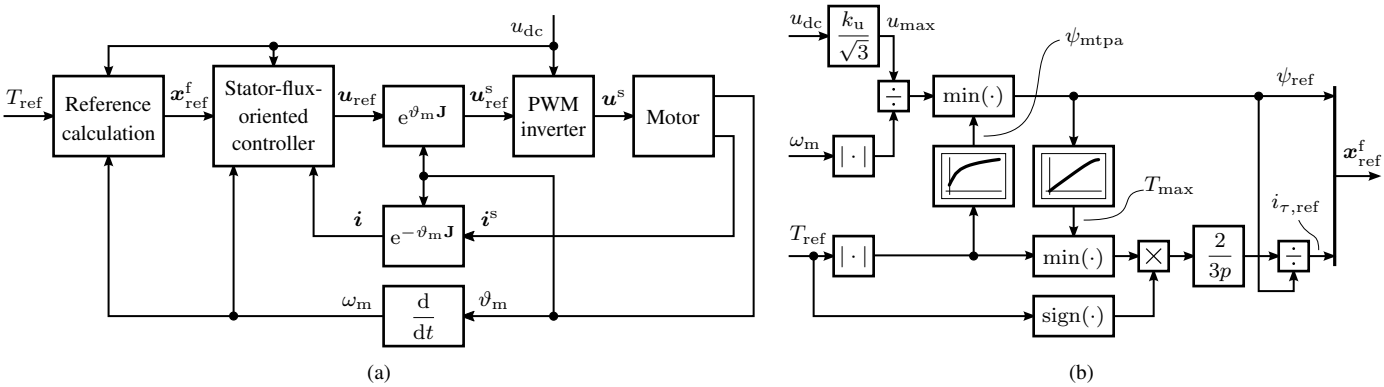

Fig. 2. Control system: (a) overall block diagram; (b) reference calculation. Vectors in stator coordinates are marked with the superscript s. In (b), one look-up table gives ψ_{mtpa} corresponding to the MTPA locus and the other gives the maximum torque T_{max} corresponding to the MTPV and current limits. The maximum steady-state voltage u_{max} is obtained from the DC-bus voltage u_{dc}. The factor k_{u} defines the voltage margin.

II. Motor Model

A. Rotor Coordinates

A standard model for the synchronous motors is used, expressed using real space vectors. As an example, the stator flux linkage in rotor coordinates is denoted by $\boldsymbol{\psi} = [\psi_{\mathrm{d}}, \psi_{\mathrm{q}}]^{\mathrm{T}}$, where ψ_{d} and ψ_{q} are the direct and quadrature components, respectively. The stator voltage equation is

$$\frac{\mathrm{d}\boldsymbol{\psi}}{\mathrm{d}t} = \boldsymbol{u} - R\boldsymbol{i} - \omega_{\mathrm{m}}\mathbf{J}\boldsymbol{\psi} \tag{1}$$

where $\boldsymbol{u}$ is the stator voltage, $\boldsymbol{i}$ is the stator current, R is the stator resistance, ω_{m} is the electrical angular speed of the rotor, and $\mathbf{J} = \left[\begin{smallmatrix} 0 & -1 \\ 1 & 0 \end{smallmatrix}\right]$ is the orthogonal rotation matrix. The stator flux is

$$\boldsymbol{\psi} = \boldsymbol{L}\boldsymbol{i} + \boldsymbol{\psi}_{\mathrm{f}} \tag{2}$$

The inductance matrix and the PM-flux vector, respectively, are

$$\boldsymbol{L} = \begin{bmatrix} L_{\mathrm{d}} & 0 \\ 0 & L_{\mathrm{q}} \end{bmatrix} \qquad \boldsymbol{\psi}_{\mathrm{f}} = \begin{bmatrix} \psi_{\mathrm{f}} \\ 0 \end{bmatrix} \tag{3}$$

where L_{d} is the d-axis inductance, L_{q} is the q-axis inductance, and ψ_{f} is the flux linkage induced due to the PMs. If $L_{\mathrm{d}} = L_{\mathrm{q}}$, the model represents the surface-mounted PM motor. If $\psi_{\mathrm{f}} = 0$, the model of the SyRM is obtained. The electromagnetic torque can be written as

$$T = \frac{3p}{2}\boldsymbol{i}^{\mathrm{T}}\mathbf{J}\boldsymbol{\psi} = \frac{3p}{2}(\psi_{\mathrm{d}} i_{\mathrm{q}} - \psi_{\mathrm{q}} i_{\mathrm{d}}) \tag{4}$$

where p is the number of pole pairs.

B. Stator-Flux Coordinates

Fig. 1 shows stator-flux coordinates ($\psi\tau$), whose ψ-axis is parallel to the stator flux. The vectors in these coordinates are marked with the superscript f, e.g.,

$$\boldsymbol{\psi}^{\mathrm{f}} = \begin{bmatrix} \psi \\ 0 \end{bmatrix} = \mathrm{e}^{-\delta\mathbf{J}}\boldsymbol{\psi} \qquad \boldsymbol{i}^{\mathrm{f}} = \begin{bmatrix} i_\psi \\ i_\tau \end{bmatrix} = \mathrm{e}^{-\delta\mathbf{J}}\boldsymbol{i} \tag{5}$$

where δ is the angle of the stator flux vector in rotor coordinates.[1] Other vectors are transformed to stator-flux coordinates similarly. In stator-flux coordinates, the torque expression (4) reduces to

$$T = \frac{3p}{2}\psi i_\tau \tag{6}$$

As explained later, the reference calculation becomes simple, if the stator flux linkage and the torque-producing current component are used as the controlled state variables. These variables are packed into a state vector

$$\boldsymbol{x}^{\mathrm{f}} = \begin{bmatrix} \psi \\ i_\tau \end{bmatrix} \tag{7}$$

Using (1), (2), and (5), a nonlinear model with the desired state variables is obtained [6]

$$\frac{\mathrm{d}\boldsymbol{x}^{\mathrm{f}}}{\mathrm{d}t} = \begin{bmatrix} 1 & 0 \\ a/L_{\mathrm{d}} & b/L_{\mathrm{d}} \end{bmatrix} \left(\boldsymbol{u}^{\mathrm{f}} - R\boldsymbol{i}^{\mathrm{f}} - \omega_{\mathrm{m}}\mathbf{J}\boldsymbol{\psi}^{\mathrm{f}} \right) \tag{8}$$

where the factors are

$$\begin{aligned} a &= \frac{1}{2}\left(\frac{L_{\mathrm{d}}}{L_{\mathrm{q}}} - 1\right)\sin 2\delta \\ b &= \frac{\psi_{\mathrm{f}}}{\psi}\cos\delta + \left(\frac{L_{\mathrm{d}}}{L_{\mathrm{q}}} - 1\right)\cos 2\delta \end{aligned} \tag{9}$$

It is to be noted that $b = 0$ corresponds to the MTPV limit.

III. Control Design

A. Structure of the Control System

Fig. 2(a) shows the overall structure of the control system considered in this paper. The measured current is transformed to rotor coordinates using the electrical angular position ϑ_{m} of the rotor. The voltage reference $\boldsymbol{u}_{\mathrm{ref}}$ is transformed to stator coordinates and fed to the pulse-width modulator (PWM). The main focus of this paper is on the stator-flux-oriented controller, which controls the state variables defined in (7).

[1] For brevity, the coordinate transformations are expressed using the matrix exponential. The transformation can be written in different forms: $\exp(\delta\mathbf{J}) = \left[\begin{smallmatrix} \cos\delta & -\sin\delta \\ \sin\delta & \cos\delta \end{smallmatrix}\right]$. The matrix elements are $\cos\delta = \psi_{\mathrm{d}}/\psi$ and $\sin\delta = \psi_{\mathrm{q}}/\psi$, where the flux magnitude is $\psi = (\psi_{\mathrm{d}}^2 + \psi_{\mathrm{q}}^2)^{1/2}$.

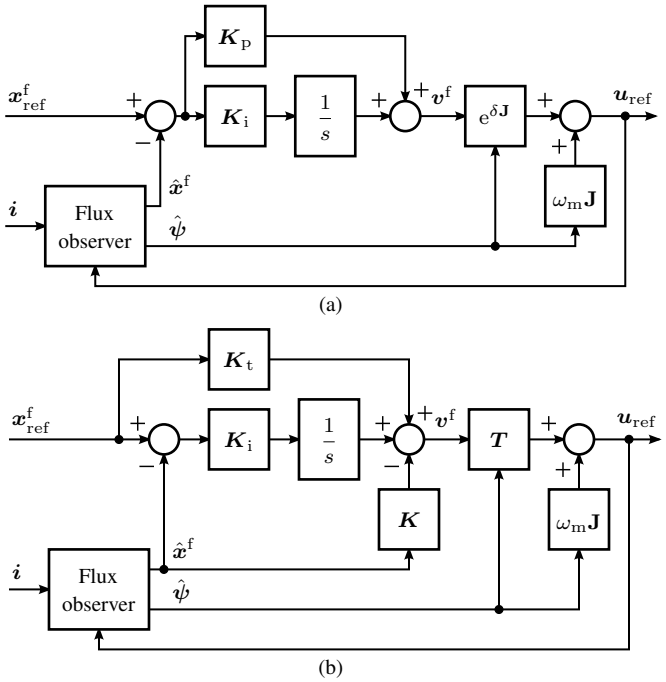

Fig. 3. Stator-flux-oriented controller: (a) conventional method; (b) proposed method. The nonlinear transformation matrix $\boldsymbol{T} = \boldsymbol{T}(\boldsymbol{\psi})$ is given in (18). Here, the flux observer operates in rotor coordinates, but stator coordinates could be used as well. The compensation for the resistive voltage drop has been omitted. The anti-windup is not shown in these figures.

This choice of the state variables is advantageous since the optimal reference $\boldsymbol{x}^\mathrm{f}_\mathrm{ref} = [\psi_\mathrm{ref}, i_{\tau,\mathrm{ref}}]^\mathrm{T}$ is comparatively easy to calculate from the torque reference T_ref, measured speed ω_m, and measured DC-bus voltage u_dc. Fig. 2(b) shows an example method for reference calculation. Due to its feedforward nature, the dynamics of the inner control loop remain intact and the noise content in the state references is minor. The MTPA and MTPV tables can be computed automatically, if the magnetic model of the motor is known [4]. Other similar reference calculation schemes are also available [6], [7].

The reference calculation method in Fig. 2(b) can be used together in current-controlled drives as well [1], [4]. However, one or two additional two-dimensional look-up tables (depending on the implementation) are needed for transforming $\boldsymbol{x}^\mathrm{f}_\mathrm{ref}$ to the corresponding optimal current reference $\boldsymbol{i}_\mathrm{ref}$. This additional complexity is avoided in the stator-flux-oriented control.

It is worth noticing that the MTPV limit as well as zero stator-flux magnitude condition are singularities in stator-flux oriented control. Therefore, some small margin (e.g. $5\ldots10\%$) in the MTPV limit as well as some small minimum value for ψ_ref are needed in the implementation. In the case of the current-controlled drives, these singularities do not exist.

B. Conventional Stator-Flux-Oriented Controller

Fig. 3(a) shows a conventional stator-flux-oriented controller similar to [6], [7]. Its two key elements, a flux observer and a proportional-integral (PI) controller are briefly reviewed in the following. An ideal PWM inverter is assumed, $\boldsymbol{u} = \boldsymbol{u}_\mathrm{ref}$.

1) Flux Observer: The stator-flux-oriented controller needs an estimate of the stator flux $\boldsymbol{\psi}$. The flux can be estimated directly using the flux model (2) without any observer. Then, the state vector $\boldsymbol{x}^\mathrm{f}$ is obtained using (5) and (7). An advantage of this approach is that the order of the whole control system is not increased due to the flux estimation and no additional gains are needed.

Applying a flux observer is preferred in practice, since it reduces the sensitivity to the errors in the magnetic model (2) and to the measurement noise. If the drive is equipped with a position sensor, the flux linkage can be estimated using a simple state observer in rotor coordinates,

$$\frac{\mathrm{d}\hat{\boldsymbol{\psi}}}{\mathrm{d}t} = \boldsymbol{u} - R\boldsymbol{i} - \omega_\mathrm{m}\mathbf{J}\hat{\boldsymbol{\psi}} + \boldsymbol{G}(\boldsymbol{L}\boldsymbol{i} + \boldsymbol{\psi}_\mathrm{f} - \hat{\boldsymbol{\psi}}) \qquad (10)$$

where $\boldsymbol{G}$ is the observer gain matrix. Based on (1), (2), and (10), the dynamics of the estimation error $\tilde{\boldsymbol{\psi}} = \boldsymbol{\psi} - \hat{\boldsymbol{\psi}}$ are governed by

$$\frac{\mathrm{d}\tilde{\boldsymbol{\psi}}}{\mathrm{d}t} = -\left(\omega_\mathrm{m}\mathbf{J} + \boldsymbol{G}\right)\tilde{\boldsymbol{\psi}} \qquad (11)$$

Therefore, any desired closed-loop system matrix can be easily set via the observer gain $\boldsymbol{G}$. If a constant gain matrix $\boldsymbol{G} = g\mathbf{I}$ is used, the observer behaves as the voltage model at higher speeds and as the flux model at low speeds [10]. The parameter g defines the corner frequency (typically $g = 2\pi \cdot 15\ldots30$ rad/s). The flux observer (10) is presented here as an example, but other flux observers could be used instead. Motion-sensorless observers are reviewed in [11].

2) PI Controller: The voltage reference in rotor coordinates is

$$\boldsymbol{u}_\mathrm{ref} = R\boldsymbol{i} + \omega_\mathrm{m}\mathbf{J}\boldsymbol{\psi} + \mathrm{e}^{\delta\mathbf{J}}\boldsymbol{v}^\mathrm{f} \qquad (12)$$

The output of a proportional-integral (PI) controller is

$$\boldsymbol{v}^\mathrm{f} = \left(\boldsymbol{K}_\mathrm{p} + \frac{\boldsymbol{K}_\mathrm{i}}{s}\right)\left(\boldsymbol{x}^\mathrm{f}_\mathrm{ref} - \boldsymbol{x}^\mathrm{f}\right) \qquad (13)$$

where $s = \mathrm{d}/\mathrm{d}t$ is used as the differential operator. The gain matrices are

$$\boldsymbol{K}_\mathrm{p} = \begin{bmatrix} k_{\mathrm{p}\psi} & 0 \\ 0 & k_{\mathrm{p}\tau} \end{bmatrix} \qquad \boldsymbol{K}_\mathrm{i} = \begin{bmatrix} k_{\mathrm{i}\psi} & 0 \\ 0 & k_{\mathrm{i}\tau} \end{bmatrix} \qquad (14)$$

where $k_{\mathrm{p}\psi}$ and $k_{\mathrm{i}\psi}$ are the gains for the flux channel and $k_{\mathrm{p}\tau}$ and $k_{\mathrm{i}\tau}$ are the gains for the torque channel. The effect of the compensation for the resistive voltage drop in (12) is small and it can be omitted due to the integral action in (13). This controller is illustrated in Fig. 3(a).

Typically, constant gains in (14) are used. As mentioned, the motor model in (8) is nonlinear and the dynamics of i_τ depend strongly on b [6]. Therefore, the control response for constant gains depends on the operating point.

C. Proposed Stator-Flux-Oriented Controller

Fig. 3(b) shows the proposed stator-flux-oriented controller, which will be explained in the following. The same flux observer as in the conventional method can be used.

1) Nonlinear State Feedback: We apply exact input-output feedback linearization [12] to tackle the nonlinearity in the model (8). Inserting the control law

$$\boldsymbol{u}^{\mathrm{f}} = R\boldsymbol{i}^{\mathrm{f}} + \omega_{\mathrm{m}}\mathbf{J}\boldsymbol{\psi}^{\mathrm{f}} + \begin{bmatrix} 1 & 0 \\ -a/b & L_{\mathrm{d}}/b \end{bmatrix} \boldsymbol{v}^{\mathrm{f}} \tag{15}$$

into (8) leads to a simple linear system

$$\frac{\mathrm{d}\boldsymbol{x}^{\mathrm{f}}}{\mathrm{d}t} = \boldsymbol{v}^{\mathrm{f}} \tag{16}$$

where $\boldsymbol{v}^{\mathrm{f}}$ is the transformed input vector, obtained from an external linear controller to be designed in the following. Since the voltage inputs u_ψ and u_τ appear in the outputs ψ and i_τ in (5) after one differentation, the relative degree of both outputs is one and the total relative degree is $r = 2$. The order of the system is $n = 2$. Since $n - r = 0$, there are no zero dynamics and the system is fully input-output linearizeable [12].

The voltage reference $\boldsymbol{u}_{\mathrm{ref}}$ is obtained by transforming the control law (15) from stator-flux coordinates to rotor coordinates

$$\boldsymbol{u}_{\mathrm{ref}} = R\boldsymbol{i} + \omega_{\mathrm{m}}\mathbf{J}\boldsymbol{\psi} + \boldsymbol{T}\boldsymbol{v}^{\mathrm{f}} \tag{17}$$

where

$$\boldsymbol{T} = \mathrm{e}^{\delta\mathbf{J}} \begin{bmatrix} 1 & 0 \\ -a/b & L_{\mathrm{d}}/b \end{bmatrix} \tag{18}$$

This nonlinear transformation matrix includes both the coordinate transformation and the feedback linearization.

2) Linear Controller: The relation (16) between the transformed input and the output can be rewritten as

$$\boldsymbol{x}^{\mathrm{f}} = \boldsymbol{v}^{\mathrm{f}}/s \tag{19}$$

A linear controller can be easily designed for the system (19). A state-feedback controller with reference feedforward and integral action is used,

$$\boldsymbol{v}^{\mathrm{f}} = \boldsymbol{K}_{\mathrm{t}}\boldsymbol{x}^{\mathrm{f}}_{\mathrm{ref}} + \frac{\boldsymbol{K}_{\mathrm{i}}}{s}\left(\boldsymbol{x}^{\mathrm{f}}_{\mathrm{ref}} - \boldsymbol{x}^{\mathrm{f}}\right) - \boldsymbol{K}\boldsymbol{x}^{\mathrm{f}} \tag{20}$$

where $\boldsymbol{K}_{\mathrm{t}}$ is the reference feedforward gain, $\boldsymbol{K}_{\mathrm{i}}$ is the integral gain, and $\boldsymbol{K}$ is the state-feedback gain. The gains can be selected as $\boldsymbol{K}_{\mathrm{t}} = \alpha\mathbf{I}$, $\boldsymbol{K}_{\mathrm{i}} = \alpha^2\mathbf{I}$, and $\boldsymbol{K} = 2\alpha\mathbf{I}$, leading to the first-order closed-loop response

$$\boldsymbol{x}^{\mathrm{f}} = \frac{\alpha}{s+\alpha}\boldsymbol{x}^{\mathrm{f}}_{\mathrm{ref}} \tag{21}$$

where α is the bandwidth. If desired, the controller can be easily modified such that the flux and torque channels have different bandwidths. If desired, different linear controller structures could be used instead. As an example, a simple proportional controller suffices, if steady-state errors are acceptable.

3) Implementation Aspects: So far, we have assumed an ideal inverter, $\boldsymbol{u} = \boldsymbol{u}_{\mathrm{ref}}$. However, the inverter output voltage is limited. Fig. 4 illustrates the maximum available voltage, which corresponds to the border of the voltage hexagon. In the first sector, the maximum voltage magnitude is [13]

$$u_{\max} = \frac{u_{\mathrm{dc}}}{\sqrt{3}\sin(2\pi/3 - \vartheta_{\mathrm{u}})} \tag{22}$$

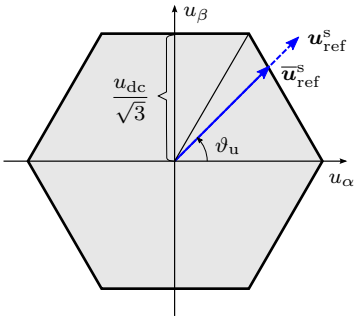

Fig. 4. Voltage hexagon of a two-level PWM inverter in stator coordinates.

TABLE I
DATA OF THE 6.7-KW SYRM

Rated values		
Phase voltage (peak value)	$\sqrt{2/3}\cdot$370 V	1.00 p.u.
Current (peak value)	$\sqrt{2}\cdot$15.5 A	1.00 p.u.
Frequency	105.8 Hz	1.00 p.u.
Speed	3175 r/min	1.00 p.u.
Torque	20.1 Nm	0.67 p.u.
Parameters at the rated operating point		
d-axis inductance L_{d}	45.6 mH	2.20 p.u.
q-axis inductance L_{q}	6.84 mH	0.33 p.u.
Stator resistance R	0.55 Ω	0.04 p.u.
PM flux ψ_{f}	0	0

where $\vartheta_{\mathrm{u}} = [0, \pi/3]$ is the angle of the voltage reference $\boldsymbol{u}^{\mathrm{s}}_{\mathrm{ref}}$. This equation can be easily applied in other sectors as well. The realizable voltage reference can be calculated as

$$\overline{\boldsymbol{u}}_{\mathrm{ref}} = \begin{cases} \boldsymbol{u}_{\mathrm{ref}}, & \text{if } \|\boldsymbol{u}_{\mathrm{ref}}\| \le u_{\max} \\ \dfrac{\boldsymbol{u}_{\mathrm{ref}}}{\|\boldsymbol{u}_{\mathrm{ref}}\|}u_{\max}, & \text{if } \|\boldsymbol{u}_{\mathrm{ref}}\| > u_{\max} \end{cases} \tag{23}$$

The realizable voltage can be either calculated in the controller using (22) and (23) or it can be obtained from the PWM.

In practice, the control system is implemented in a digital computer. The PWM can be modeled as a zero-order hold in stator coordinates. Furthermore, the control system has typically a computational delay of one sampling period. Fig. 5 shows a discrete-time implementation, where the PWM and computational delays are compensated for [3], [14] and the inverter voltage saturation is taken into account by means of an anti-windup mechanism based on the realizable voltage reference [15].

IV. RESULTS

The conventional and proposed stator-flux-oriented control schemes are evaluated using simulations and experiments. The control system was implemented on a dSPACE DS1006 processor board. The studied motor is a transverse-laminated 6.7-kW four-pole SyRM, whose rated data are given in Table I. The effects of the magnetic saturation are taken into account in the control system by replacing the flux model in (2) with an algebraic magnetic model [16]. A single-update PWM is used and the sampling (switching) frequency is 5 kHz. The stator currents and the DC-link voltage are measured

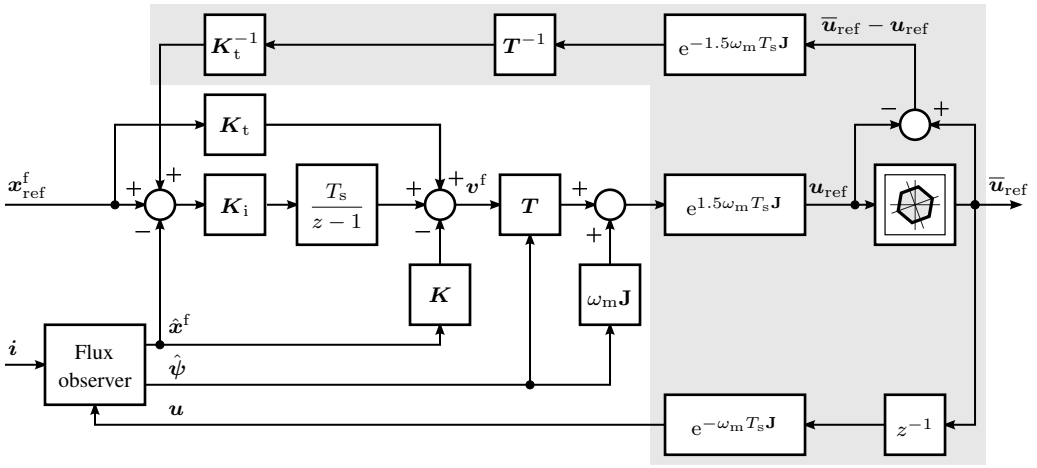

Fig. 5. Discrete-time stator-flux-oriented controller. The sampling period is denoted by T_s. In the shaded region, the anti-windup mechanism and the compensations for the PWM and computational delays are shown. This structure is valid also for the conventional method, if $\boldsymbol{T} = \exp(\delta\mathbf{J})$ and $\boldsymbol{K}_\mathrm{t} = \boldsymbol{K} = \boldsymbol{K}_\mathrm{p}$ are used.

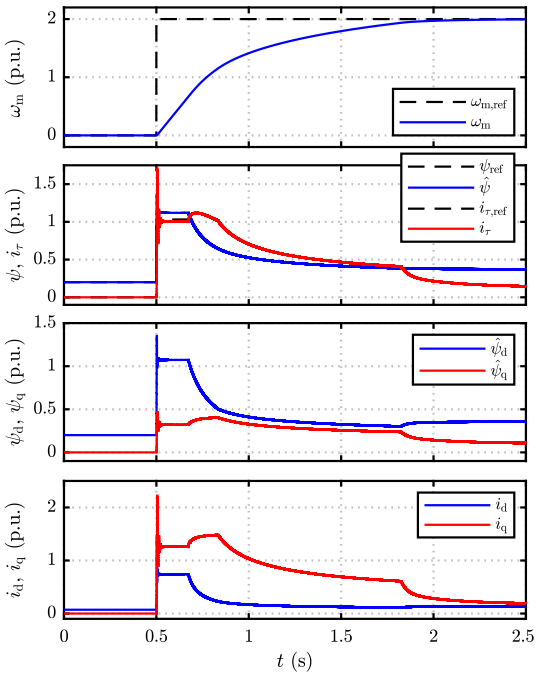

Fig. 6. Simulation results for the conventional controller. Acceleration from zero to the speed of 2 p.u. First subplot: actual speed and its reference. Second subplot: controlled variables and their references. Third subplot: estimated flux components. Last subplot: measured current components.

in synchronism with the PWM. The rotor speed is measured using an incremental encoder. A servo induction machine is used as a loading machine.

The control scheme shown in Fig. 2 is augmented with a speed controller, which provides the torque reference T_ref based on the speed reference $\omega_\mathrm{m,ref}$ and the measured speed ω_m. The current limit is 1.5 p.u. Here, the results are only shown for the stator-flux-oriented controller with the flux observer (10). The variant without the observer performs similarly, with the exception of slightly more noise in the controlled variables.

A. Conventional Controller

A conventional stator-flux-oriented controller is considered. The control structure shown in Fig. 5 is parametrized to equal the conventional scheme: $\boldsymbol{T} = \exp(\delta\mathbf{J})$ and $\boldsymbol{K}_\mathrm{t} = \boldsymbol{K} = \boldsymbol{K}_\mathrm{p}$. The gains in (14) are: $k_{\mathrm{p}\psi} = 2\,500$ rad/s, $k_{\mathrm{i}\psi} = 625$ (rad/s)^2, $k_{\mathrm{p}\tau} = 12 \cdot 10^3$ V/A, and $k_{\mathrm{i}\tau} = 3\,000$ V/(As). According to [6], these gains correspond to the following best-case design bandwidths: $2\pi \cdot 400$ rad/s for the flux channel and $2\pi \cdot 75$ rad/s for the current channel.

Fig. 6 shows the simulation results of an acceleration test, where the speed reference is changed stepwise from 0 to 2 p.u. The large overshoot and oscillations can be seen in the torque-producing current i_τ after the speed reference changes at $t = 0.5$ s. The control performance could be improved by means of scheduling the controller gains as a function of the operating point. However, the gain scheduling would be a difficult and time-consuming process, if done by means of the trial-and error method.

B. Proposed Controller

1) Acceleration Test: In the following, the bandwidth is $\alpha = 2\pi \cdot 100$ rad/s. Fig. 7 shows results of the acceleration test: the simulation results are shown in Fig. 7(a) and the experimental results in Fig. 7(b). The controlled variables follow their references according to the designed closed-loop dynamics, cf. (21). It can also be seen that the experimental results match very well with the simulation results.

2) Constant Speed Test: Fig. 8 shows the results when the speed of the load drive is regulated at 0.5 p.u. and the drive under test is controlled in the torque-control mode: the simulation results are shown in Fig. 8(a) and the experimental results in Fig. 8(b). The torque reference is stepped from zero to the rated torque with increments of 25% of the rated torque. The controlled variables follow properly their references. The

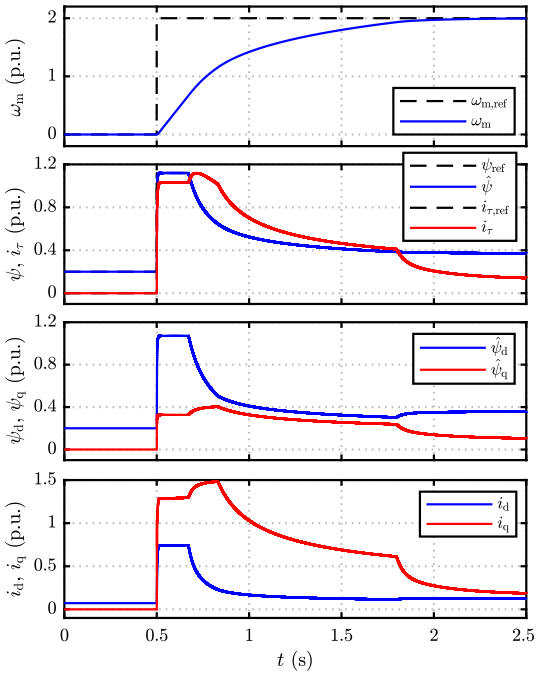

(a)

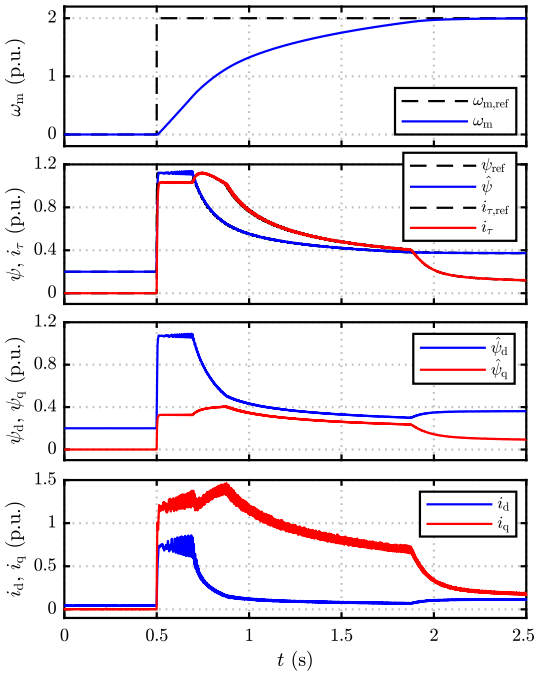

(b)

Fig. 7. Acceleration from zero to the speed of 2 p.u.: (a) simulation results; (b) experimental results. First subplot: actual speed and its reference. Second subplot: controlled variables and their references. Third subplot: estimated flux components. Last subplot: measured current components.

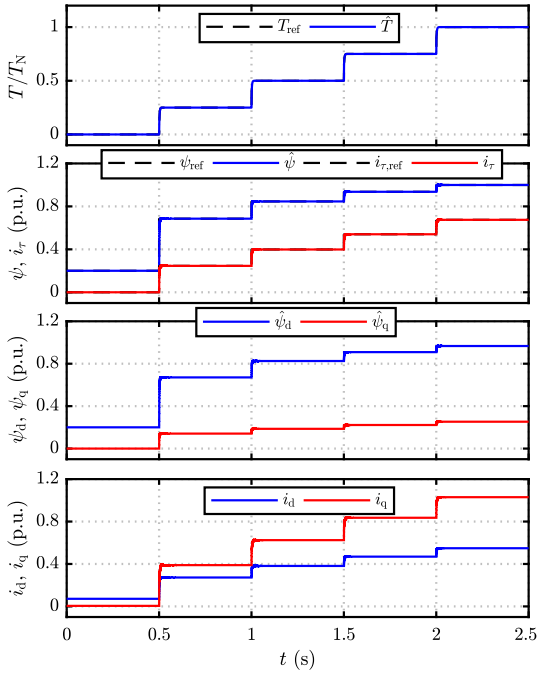

(a)

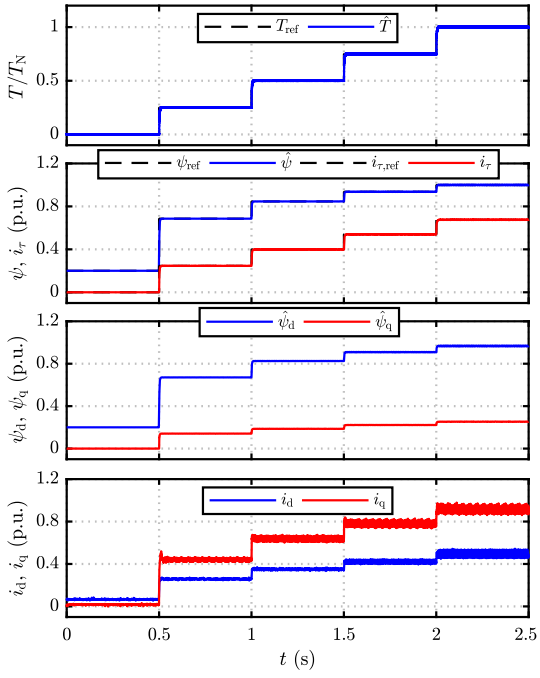

(b)

Fig. 8. Torque reference steps at the speed of 0.5 p.u.: (a) simulation results; (b) experimental results. First subplot: reference and estimated torque $\hat{T} = (3/2)p\hat{\psi}i_\tau$. Second subplot: reference and estimated states. Third subplot: estimated flux components. Last subplot: measured current components.

estimated torque and the measured current components are also shown.

V. Conclusions

We have presented a systematic design procedure for a decoupled stator-flux-oriented control method for synchronous motors. A comparison is presented between the conventional and the proposed controller. Furthermore, we have shown that the proposed method can be implemented without an observer (but the observer typically improves the control performance and robustness and is therefore recommended). For implementation purposes, the discrete-time equivalent of the proposed controller and anti-windup mechanism is also presented. Further, the stator-flux-oriented control makes it possible to use comparatively simple reference calculation schemes. The performance of the proposed controller has been verified using simulations and experiments on a 6.7-kW SyRM drive.

Acknowledgment

The authors gratefully acknowledge ABB Oy for the financial support.

References

[1] M. Meyer and J. Böcker, "Optimum control for interior permanent magnet synchronous motors (IPMSM) in constant torque and flux weakening range," in *Proc. EPE-PEMC*, Portoroz, Slovenia, Aug./Sept. 2006, pp. 282–286.

[2] W. Peters, O. Wallscheid, and J. Böcker, "Optimum efficiency control of interior permanent magnet synchronous motors in drive trains of electric and hybrid vehicles," in *Proc. EPE ECCE-Europe*, Geneva, Switzerland, Sept. 2015.

[3] M. Hinkkanen, H. A. A. Awan, Z. Qu, T. Tuovinen, and F. Briz, "Current control for synchronous motor drives: direct discrete-time pole-placement design," *IEEE Trans. Ind. Appl.*, vol. 52, no. 2, pp. 1530–1541, Mar./Apr. 2016.

[4] H. A. A. Awan, Z. Song, S. E. Saarakkala, and M. Hinkkanen, "Optimal torque control of synchronous motor drives: Plug-and-play method," in *Proc. IEEE ECCE*, Cincinnati, OH, Oct. 2017, pp. 334–341.

[5] H. F. Hofmann, S. R. Sanders, and A. EL-Antably, "Stator-flux-oriented vector control of synchronous reluctance machines with maximized efficiency," *IEEE Trans. Ind. Electron.*, vol. 51, no. 5, pp. 1066–1072, Oct. 2004.

[6] G. Pellegrino, E. Armando, and P. Guglielmi, "Direct flux field-oriented control of IPM drives with variable DC link in the field-weakening region," *IEEE Trans. Ind. Appl.*, vol. 45, no. 5, pp. 1619–1627, Sept./Oct. 2009.

[7] ——, "Direct-flux vector control of IPM motor drives in the maximum torque per voltage speed range," *IEEE Trans. Ind. Electron.*, vol. 59, no. 10, pp. 3780–3788, Oct. 2012.

[8] M. Bilewski, A. Fratta, L. Giordano, A. Vagati, and F. Villata, "Control of high-performance interior permanent magnet synchronous drives," *IEEE Trans. Ind. Appl.*, vol. 29, no. 2, pp. 328–337, Mar. 1993.

[9] S. Ekanayake, R. Dutta, M. F. Rahman, and D. Xiao, "Direct torque and flux control of interior permanent magnet synchronous machine in deep flux-weakening region," *IET Electr. Power Appl.*, vol. 12, no. 1, pp. 98–105, Jan. 2018.

[10] P. Guglielmi, M. Pastorelli, G. Pellegrino, and A. Vagati, "Position-sensorless control of permanent-magnet-assisted synchronous reluctance motor," *IEEE Trans. Ind. Appl.*, vol. 40, no. 2, pp. 615–622, Mar./Apr. 2004.

[11] M. Hinkkanen, S. E. Saarakkala, H. A. A. Awan, E. Mölsä, and T. Tuovinen, "Position estimation for synchronous motor drives: Unified framework for design and analysis," in *Proc. IEEE SLED*, Catania, Italy, Sept. 2017, pp. 25–30.

[12] S. S. Sastry and A. Isidori, "Adaptive control of linearizable systems," *IEEE Trans. Autom. Control*, vol. 34, no. 11, pp. 1123–1131, Nov. 1989.

[13] A. M. Khambadkone and J. Holtz, "Compensated synchronous PI current controller in overmodulation range and six-step operation of space-vector-modulation based vector-controlled drives," *IEEE Trans. Ind. Electron.*, vol. 49, no. 3, pp. 574–580, Jun. 2002.

[14] B.-H. Bae and S.-K. Sul, "A compensation method for time delay of full-digital synchronous frame current regulator of PWM AC drives," *IEEE Trans. Ind. Appl.*, vol. 39, no. 3, pp. 802–810, May/June 2003.

[15] Y. Peng, D. Vrancic, and R. Hanus, "Anti-windup, bumpless, and conditioned transfer techniques for PID controllers," *IEEE Control Syst. Mag.*, vol. 16, no. 4, pp. 48–57, Aug. 1996.

[16] M. Hinkkanen, P. Pescetto, E. Mölsa, S. E. Saarakkala, G. Pellegrino, and R. Bojoi, "Sensorless self-commissioning of synchronous reluctance motors at standstill without rotor locking," *IEEE Trans. Ind. Appl.*, vol. 53, no. 3, pp. 2120–2129, May/June 2017.